Journal of Chemical&Engineering Data

pubs.acs.org/jced Article

Thermal Conductivity of 1-Alkyl-3-methylimidazolium [Tf_2N] Ionic Liquids and Compressed 1,1,1,2-Tetrafluoroethane (R-134a)

Karim S. Al-Barghouti and Aaron M. Scurto*

Cite This: https://doi.org/10.1021/acs.jced.2c00054 Read Online

ACCESS | Metrics & More | Article Recommendations | Supporting Information

ABSTRACT: The thermal conductivities of mixtures of ionic liquids (ILs) and fluorocarbon gases are necessary for the design of a variety of engineering and separation applications. Here, a transient hot-wire technique was used to measure the liquid thermal conductivities of 1-ethyl-3-methylimidazolium bis-(trifluoromethylsulfonyl)amide ([EMIm][Tf_2N]) and 1-*n*-hexyl-3-methylimidazolium bis(trifluoromethylsulfonyl)amide ([HMIm][Tf_2N]) in vapor−liquid equilibrium with the hydrofluorocarbon gas, 1,1,1,2-tetrafluoroethane (R-134a), at (298.15, 323.15, 348.15) K for [HMIm][Tf_2N] and (298.15, 348.15, 398.15) K for [EMIm][Tf_2N] and pressures up to 28 bar. The thermal conductivity of the gas-saturated ionic liquid exhibits a very small and relatively linear decrease with increasing pressure (composition) of R-134a even to relatively high compositions (~80% mol). Only at very high molar compositions of the gas (~90+% mol) does the thermal conductivity significantly decrease toward that of the value of pure saturated liquid R-134a. However, no simple mixing rule of the pure component properties could correlate the trends in composition. As some potential applications require higher temperatures, the system of [EMIm][Tf_2N]/R-134a was measured at 398.15 K. Generally, a longer alkyl-chain length on the cation, such as [HMIm][Tf_2N], experiences a steeper decrease in thermal conductivity with increasing R-134a composition than with the [EMIm] cation.

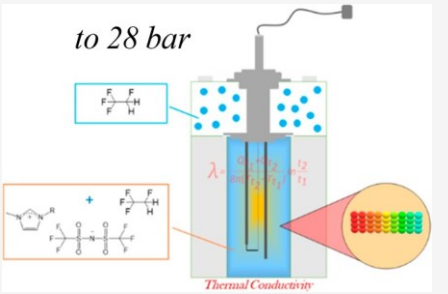

1. INTRODUCTION

Ionic liquids (ILs) have gained increasing attention as potential substitutes for common solvents and engineering fluids in a myriad of potential applications. They possess unique properties including low to negligible volatility and decreased vapor pollution relative to other volatile organic solvents. Various cationic and anionic combinations in ILs allow for tunable properties such as miscibility, hydrophobicity or hydrophilicity, solvation, polarity, and varying transport properties as well as reactive properties.[1,2] The selective tunability of ILs allows for their potential use in various fields including catalysis,[3−5] gas separations,[6−16] energy storage and fuel cells,[17−21] refrigeration systems and heat transformers,[22−25] etc.

Coupling ionic liquids with refrigerant gases has been proposed for absorption refrigeration.[22−29] Here, the IL dissolves the refrigerant gas in one stage and is pumped to a higher pressure, heat is added to liberate a high-pressure gas, and the gas is cooled and condensed to a liquid and finally depressurized to produce the refrigeration effect. As the IL is non-volatile, the gas that boils out of the IL phase is pure and does not require further equipment, i.e., a rectifier, to remove the IL from the vapor phase. To design this type of process, both thermodynamic and transport properties are required to properly model pumping duty, heat transfer rate and area, etc.[30]

In recent years, gas separations using ionic liquids have gained increased interest. Ionic liquids have been proposed as an effective medium in combatting greenhouse gases through techniques of gas capture and gas-mixture separations.[31−41] While carbon dioxide contributes to nearly 80% of greenhouse gas emissions in the United States, other gases have relatively high emission rates as well; some of the more potent greenhouse gases emitted include fluorinated gases in an emission abundance of nearly 3% (data reported in 2019).[42] Fluorinated gases are commonly utilized as refrigerants, propellants, fire retardants, and foam blowing agents.[43,44] The high global warming potential (GWP) of some commonly used fluorinated gases has called for their capture, separation, recycle, or destruction.[45] Many of the hydrofluorocarbons (HFCs) that were used to replace ozone-depleting chlorofluorocarbons (CFCs) and hydrochlorofluorocarbons (HCFCs), due to the Montreal Protocol, have high global warming potential (GWP) and are now the subject of increased concern and regulation. The Kigali Amendment to the Montreal Protocol in 2016 called for the reduction of usage and production of most HFCs by more than 80% over the next 30 years.[45,46]

Fluorocarbon gases compose 83% of refrigerant gases used for refrigeration and air-conditioning worldwide and 32% of

Special Issue: In Honor of Joan F. Brennecke

Received: January 25, 2022
Accepted: July 8, 2022

Table 1. Specifications of Chemicals

Chemical Name	Chemical Structure	CAS no.	Source	Purity (%mol)	Water Content (ppm)[c]	Purification Method
1-n-Hexyl-3-methyl-imidazolium bis[(trifluoromethyl)sulfonyl]amide ([HMIm][Tf_2N])	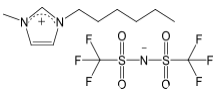	382150-50-7	IoLiTec	99+%[a]	<130	Vacuum Drying
1-Ethyl-3-methyl-imidazolium bis[(trifluoromethyl)sulfonyl]amide ([EMIm][Tf_2N])	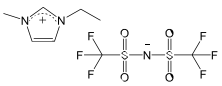	174899-82-2	IoLiTec	99+%[a]	<130	Vacuum Drying
1,1,1,2-Tetrafluoroethane (R-134a)		811-97-2	ASPEN Refrigerants	99.99%[b]	N/A	N/A

[a]Reported by manufacturer and confirmed here by NMR analysis after purification. [b]Specified by supplier. [c]Mass basis.

gases used in foam blowing.[47] Commonly used pure component refrigerants include R-134a (1,1,1,2-tetrafluoroethane), R-32 (difluoromethane), and R-22 (chlorodifluoromethane, an HCFC). R-134a and R-32, alongside other pure HFC refrigerants in different combinations, are common constituents of widely used HFC blends such as R-410A (R-32 and R-125), R-404A (R-125, R-143a, R-134a), and R-407C (R-32, R-125, R-134a). Most HFC blends form azeotropic or near azeotropic mixtures that render separation and recycling as non-trivial processes. Not all HFCs require immediate phase out; for instance, R-32 (difluoromethane) has a low enough GWP for continued use in some jurisdictions.[48,49] Thus, separating the gases from blends that can be recycled or used in future applications will be an important process in the future.

Ionic liquids have been proposed to help separate many of these HFC mixtures.[15,16,34,41,50,51] Extractive distillation has been suggested to circumvent the azeotrope or aid in difficult separations. The design of these types of systems requires extensive knowledge of both thermodynamic and transport properties. Extensive phase equilibria thermodynamic studies have been conducted on systems of varying ILs and fluorinated gases.[50−54] Much less research has been devoted to mass and momentum transport properties. We and other groups have begun measuring the viscosity and diffusivity in IL/gas systems.[55,56]

Mixture heat transport properties of IL systems are very scarce in the literature. Such properties would be necessary for optimal design and sizing of engineering components utilizing IL/gas mixtures such as heat exchangers, reboilers, etc. Limited studies report on the thermal conductivities of pure IL systems using varying techniques.[57−75] Commonly utilized techniques for measuring and predicting the thermal conductivity of ILs include the transient hot-wire method, the guarded parallel-plate method, molecular dynamic simulations, and transient grating techniques. Thermal conductivity values of refrigerant gases and liquids are reported with widespread use in industry.[76−78] Tomida et al. reports on the thermal conductivity data of subsaturated CO_2/IL systems at temperatures ranging from 294 K to 334 K and mole fractions of CO_2 up to 0.42 in the ILs, 1-butyl-3-methylimidazolium hexafluorophosphate ([BMIm][PF_6]) and 1-butyl-3-methylimidazolium tetrafluoroborate ([BMIm][BF_4]).[79] Rausch et al.[80] and Klein et al.[81] measured the thermal diffusivities (related to thermal conductivity by mixture density and heat capacity) of several ILs under different conditions with various dissolved gases utilizing a dynamic light scattering technique and molecular dynamics simulations (Klein et al.[81]). We have previously utilized a transient hot-wire method to measure and report thermal properties, including thermal conductivity, of CO_2-expanded *n*-alkanes.[82] More recently, we have reported thermal conductivity data for an ionic liquid saturated with compressed CO_2 over three isotherms (298.15, 323.15, 348.15) K.[83]

1,1,1,2-Tetrafluoroethane (R-134a) is a prevalent HFC found in many commercial, home, and vehicle cooling systems. R-134a has been proposed as a potential gas for an IL-based air-conditioning system and is found in a number of refrigerant mixtures that require future separation (see above). We have previously investigated the phase behavior and solubility of R-134a in different imidazolium-based ionic liquids at temperatures of (298.15, 323.15, 348.15) K and varying pressures.[84,85] We have also reported data on the viscosity and self-diffusivity of pure ILs as well as ILs saturated with compressed gases, such as R-134a, at varying pressures and temperatures.[55,86,87] This study reports the liquid thermal conductivity values of biphasic systems of [EMIm][Tf_2N] and 1-*n*-hexyl-3-methylimidazolium [Tf_2N] ([HMIm][Tf_2N]) (see Table 1) saturated with the hydrofluorocarbon gas, R-134a, at three isotherms (298.15, 323.15, 348.15) K for [HMIm][Tf_2N] and (298.15, 348.15, 398.15) K for [EMIm][Tf_2N] and pressure up to 28 bar. The thermal conductivity of pure 1-ethyl-3-methylimidazolium bis(trifluoromethylsulfonyl)amide ([EMIm][Tf_2N]) was also measured between 298.15 K and 398.15 K.

2. EXPERIMENTAL METHODS

2.1. Thermal Conductivity. A transient hot-wire method was utilized to measure the thermal conductivity of pure ILs as well as biphasic systems of ILs/gases at equilibrium. Several groups have provided a detailed analysis on the applicability, assumptions, and principle of the methodology.[88−90] We have previously described the methodology employed herein,[82,83,91,92] but an overview of the apparatus and methodology will be provided here. A Flucon Fluid Control GmbH thermal conductivity probe and an in-house-built high-pressure equilibrium cell are utilized. The equilibrium cell sits in a heating jacket; heating fluid is circulated through the heating jacket using a Fisher Scientific Isotemp 3016 heated bath circulator with a temperature stability of ±0.01 K. A certain

https://doi.org/10.1021/acs.jced.2c00054
J. Chem. Eng. Data XXXX, XXX, XXX−XXX

amount of the IL is initially placed in the vessel; the amount initially introduced is determined based on the expected (calculated) volume expansion such that, once the mixture expands, it does not fill the entirety of the cell. The gas is introduced using a high-pressure syringe pump, Teledyne-Isco, Inc. 100DM, and the pressure in the vessel is monitored using an OMEGA DPG7000-3K pressure gauge with a range of 206.8 bar (0.05% full-scale accuracy: ±0.1 bar). The mixture is stirred using a PTFE-coated stir bar and a stir plate placed on a heavy bench to reduce vibration-induced convective effects. Pressure decay is monitored, and once the pressure is constant, stirring is stopped and the mixture is allowed to settle. Ample time is given such that all convective effects induced through stirring are dissipated. The heating bath is turned off prior to taking measurements as well to minimize all possible convective forces.

The governing equation for the thermal conductivity measurements is shown in eq 1

$$\lambda = \frac{Q_{t_1} + Q_{t_2}}{8\pi(T_{t_2} - T_{t_1})} \ln \frac{t_2}{t_1} \quad (1)$$

in which λ is the thermal conductivity of the fluid, Q is the input heat per unit length, t is time, and T is temperature. A heat input at two different times is correlated to the temperature change at the two respective times, and the thermal conductivity is obtained as shown in eq 1. The formulation and governing assumptions leading to eq 1 are omitted here but are formulated and described in detail in our previous work.[82,83] As the equations assume an infinite cylinder, end-effects are ascertained by a one-point calibration, here, using *n*-heptane. *n*-Heptane was used as a calibration fluid, since its reported thermal conductivity values near room temperature and pressure are of the same order as those of the two ILs investigated in this study;[93−98] however, the device does not mandate a calibration fluid close to the test fluids. Purification of the IL in between measurements at different temperatures and following the loading steps is completed by placing the loaded, sealed vessel under a vacuum (70 mbar) while heating to ~348.15 K for ~24 h. For measurements at 398.15 K, the heating jacket was replaced by direct electric heating in which the cell was wrapped with fiberglass insulated heating tape that is supplied with power through an in-house built temperature control box that is equipped with a safety shut-off function.

The effect of highly electrically conductive fluids has been mentioned in the literature as a possible source of error for the transient hot-wire technique for thermal conductivity.[99,100] Usually for the measurement of highly electrically conductive solutions/solvents, the use of a passivated wire is recommended. Passivation is usually accomplished by using a metal wire with an insulating metal oxide layer on the surface. Here, a platinum wire was oxidized in a furnace with air by using a slow step function of heating (2 °C/min) and holding for 1.5 h at approximately every 100 °C until 600 °C. A small portion of the top of the wire was cut off following the oxidation treatment, and the exposed cross-section of the wire was then characterized using scanning electron microscopy (Hitachi High Technologies model S4700 II cFEG SEM) and energy dispersive X-ray spectroscopy (Oxford Instruments, X-Max^N Silicon drift EDX detector). X-ray photoelectron spectroscopy (Physical Electronics PHI 5000 Versaprobe-II XPS Microprobe) was then utilized to confirm the formation and structure of the metal oxide layer on the outer surface. The results clearly show a surface coverage of the metal oxide on the wire with an inner core of pure platinum. The thermal conductivity of [EMIm][Tf_2N] at three temperatures was measured with both a passivated and non-passivated (untreated) wire, and the results are shown in Table 2. As shown, the differences are well within the uncertainty of the measurements. Many ionic liquids have relatively low electrical conductivities compared with typical aqueous electrolyte solutions[101,102] and are not enough to affect the thermal conductivity measurements. R-134a has very low electrical conductivity; thus, mixtures of the IL and R-134a are anticipated to have even lower electrical conductivity than the pure IL.

Table 2. Comparison of Sample Results for [EMIm][Tf_2N] Using a "Bare" Pt Wire versus a Passivated Pt Wire

T (K)	$\lambda_{insulated}$	$\lambda_{uninsulated}$	% deviation
298.15	131.42	131.91	0.371
303.15	130.96	131.02	0.046
313.15	129.36	129.44	0.062

2.2. Uncertainty. The thermal conductivity probe has a manufacturer reported uncertainty of ±1%. However, we have performed a number of studies to ascertain the uncertainty of the instrument at different temperature ranges. The measurement-to-measurement precision is observed to be approximately ±0.03 mW/m·K at 298.15 and 323.15 K. The precision at 348.15 K is nearly ±0.3 mW/m·K, and at 398.15 K, it is approximately ±2 mW/m·K. The run-to-run repeatability is ±0.1 mW/m·K at the three initial temperatures and ±0.5 mW/m·K at a temperature of 398.15 K. The uncertainty of the calibration fluid, *n*-heptane, from the literature sources ranges from 0.3% to 0.5%—approximately ±0.5 mW/m·K.[95−97,103] Thus, total uncertainty, as the square root of the sum of squares of the measurement-to-measurement, run-to-run, and calibration fluid, is calculated to be ±0.5 mW/m·K between 298.15 K and 323.15 K, ±0.6 mW/m·K at 348.15 K, and ±2.1 mW/m·K at 398.15 K. These uncertainties are based upon the measurement at a given temperature and pressure. Convection (generally due to vibration of the equipment (heating jacket fluid flow, stirrer, etc.)) is possibly one of the main sources of variation associated with the thermal conductivity measurements. Convection (natural or forced) generally results in measurements that are skewed toward higher thermal conductivity and are potentially more prevalent at relatively higher temperatures and gas compositions. However, we do not observe nor could not conclude that any of the data suffered from this known possibility. The associated PT100 RTD has an uncertainty of ±0.1 K. The heating bath has a stability of ±0.1 K. The electrical heating element utilized at 398.15 K has a stability of ±0.2 K. The pressure gauge has a reported uncertainty of ±0.1 bar. The effects of the uncertainties in temperature and pressure on the combined standard uncertainty of the thermal conductivity measurements are negligible (<0.01 mW/m·K each) compared to the thermal conductivity uncertainty itself. This is based upon the slope of thermal conductivity with temperature from these measurements for the pure IL and our previous work which measured the effect of hydrostatic pressure on the thermal conductivity of [HMIm][Tf_2N].[82] The literature solubility data (molar composition of R-134a) utilized has a reported average uncertainty of <0.002; however, interpolation

https://doi.org/10.1021/acs.jced.2c00054
J. Chem. Eng. Data XXXX, XXX, XXX−XXX

of the data at the pressure points investigated in this work results in higher uncertainty. To estimate the uncertainty associated with interpolation, the solubility data was fit to a second-degree polynomial that was utilized to interpolate the data and the deviation between the actual experimental data and that obtained through the interpolating polynomial was calculated. The average percent deviation for [EMIm][Tf_2N] compositions is ~5% across the entire composition range, and that of [HMIm][Tf_2N] is ~3%. The highest uncertainty in reported compositions is expected to be that accompanying the predictions at 398.15 K, as those compositions were estimated using an equation of state and not directly utilizing experimental data; however, comparison of the compositional values predicted using the two different modeling techniques shows an average percent deviation of ~3% relative to each other. We believe these predictions to be better than 5%. The uncertainty of thermal conductivity as a function of composition would be in addition to those described above which are based upon temperature and pressure.

2.3. Chemicals. Both ionic liquids, [EMIm][Tf_2N] (CAS#174899-82-2) and [HMIm][Tf_2N] (CAS#382150-50-7) (see Table 1), were purchased from Iolitec. The manufacturer reported purity is >99%. Prior to the experiments, the ILs were dried under a vacuum (70 mbar) and a temperature of ~348.15 K. The post-drying water content was measured using a Mettler Toledo C20S Karl Fisher Coulometer and determined to be less than 130 ppm for both ILs. NMR analysis was performed on both samples to confirm the purity prior to measurements; no foreign peaks were detected. R-134a gas was purchased from ASPEN Refrigerants with a manufacturer stated purity of 99.99%.

3. LIQUID COMPOSITIONS USING EQUATION OF STATE PREDICTIONS

Experimental data on the solubility of R-134a in [HMIm]-[Tf_2N] as well as in [EMIm][Tf_2N] has been previously reported.[84,104] Measurements in this work have been conducted at three isotherms for R-134a/[HMIm][Tf_2N] (298.15, 323.15, 348.15) K which correspond to the same isotherms with reported solubility data. Hence, solubility data at each isotherm was interpolated from the literature to correlate the molar composition of R-134a in the liquid phase to pressure. However, for the R-134a/[EMIm][Tf_2N] system, the measurements were conducted at 298.15 K and 323.15 K (where VLE data exists) and 398.15 K where no data exists. It was difficult to ascertain the uncertainty of the use of linear or higher order polynomial extrapolation of the solubility data to the higher temperature isotherm (398.15 K). Therefore, an equation of state model and Henry's law analysis is used to predict the equilibrium compositions at 398.15 K.

The Peng−Robinson equation of state coupled with the van der Waals one-parameter mixing rule (vdW-1) was used to model the data as follows

$$P = \frac{RT}{V - b_m} - \frac{a_m}{V(V + b_m) + b_m(V - b_m)} \tag{2}$$

in which a_m is the mixture attractive parameter and b_m is the mixture co-volume parameter.

$$a = a_c(1 + \kappa(1 - \sqrt{T_r}))^2 \tag{3}$$

$$a_c = \frac{0.45724R^2T_c^2}{P_c} \tag{4}$$

$$\kappa = 0.37464 + 1.54226\omega - 0.2699\omega^2 \tag{5}$$

$$b = \frac{0.07780RT_c}{P_c} \tag{6}$$

Mixture parameters, a_m and b_m, are computed using the vdW-1 mixing rule

$$a_m = \sum_{i=1}^{N}\sum_{j=1}^{N} x_i x_j a_{ij} \tag{7}$$

$$b_m = \sum_{i=1}^{N} x_i b_i \tag{8}$$

in which

$$a_{ij} = \sqrt{a_i a_j}(1 - k_{ij}) \quad \text{with} \quad k_{ij} = k_{ji} \tag{9}$$

The pure component critical properties and acentric factor were obtained from literature predictions. Valderrama et al.[105−107] utilized group contribution methods based on those formulated by Lydersen[108] as well as those by Joback and Reid[109] to estimate the pure component critical properties and acentric factor of [EMIm][Tf_2N]; the values of those critical properties are displayed in Table 3.

Table 3. Physical Properties of [EMIm][Tf_2N] and R-134a[a]

component	MW	T_b (K)	T_c (K)	P_c (bar)	ω
[EMIm][Tf_2N]	391.3	816.7	1249.3	32.7	0.2157
R-134a	102.0	247.1	374.20	40.6	0.3268

[a]IL data from ref 105; R-134a data from refs 93 and 110.

Solubility data from our previous work at (298.15, 323.15, 348.15) K were regressed to find optimal k_{ij} parameters across the entirety of the temperature ranges. The linear temperature functionalities of the k_{ij} parameter are as follows:

$$k_{ij} = k_{ij}^{(1)} + k_{ij}^{(2)}T \tag{10}$$

ASPEN Plus V10 (thermodynamics package) was utilized to regress the data with a maximum likelihood objective function (as experimental error was reported at each point) as well as a minimization of the least-squares method to find the optimal elements of the k_{ij} parameter.

A Henry's constant analysis was also conducted to approximate the solubility at 398.15 K, and the results were compared to those of the aforementioned EoS. The procedure for obtaining solubility approximations using Henry's constant is as follows:

The definition of Henry's constant obtained at constant temperature is[111]

$$H_i = \lim_{x_i \to 0}\left(\frac{\bar{f}_i^{V}}{x_i}\right) \tag{11}$$

where H_i is Henry's constant and $\bar{f}_i$ is the mixture liquid fugacity of the solute. At low to moderate compositions and pressures where the infinite-dilution-based activity coefficient, γ_i^*, and the pressure dependence on the Henry's constant can be neglected, the mixture liquid fugacity of the solute can be

https://doi.org/10.1021/acs.jced.2c00054
J. Chem. Eng. Data XXXX, XXX, XXX−XXX

described by a linear correlation in terms of the solute molar composition in the mixture and Henry's constant and is equal to the pure component vapor phase fugacity.

$$f_i^L(T, x) = H_i(T)x_i = f_i^V(T, P) \quad (12)$$

The vapor phase fugacity of R-134a was obtained from the REFPROP database.[93,110] The linear portion of a plot of vapor phase fugacity at the temperature and pressure of the measurement with the experimental R-134a composition at constant temperature would yield a slope defined as Henry's constant. The entire reported solubility data set at each isotherm was initially used; the fugacity at each composition point (pressure) was plotted, and the R^2 value of the linear fit was assessed. Any higher-pressure data points that would drastically decrease the R^2 value, i.e., non-linear, were omitted such that the R^2 value is to remain above 0.990. The temperature dependence on the Henry's constants[112] is related to the infinite-dilution partial molar enthalpy ($\overline{\Delta_{sol}H_i^{\infty}}$) and entropy ($\overline{\Delta_{sol}S_i^{\infty}}$) of a solution, as shown in eqs 13 and 14.

$$\frac{\overline{\Delta_{sol}H_i^{\infty}}}{R} = \left\{\frac{\partial \ln H_i}{\partial\left(\frac{1}{T}\right)}\right\}_P \quad (13)$$

$$\frac{-\overline{\Delta_{sol}S_i^{\infty}}}{R} = \left\{\frac{\partial \ln H_i}{\partial \ln T}\right\}_P \quad (14)$$

The heat of solution is expected to vary only slightly with the temperature in the range considered. Equation 13 can be integrated to extrapolate to higher temperatures (T_2 = 398.15 K)

$$\frac{H_i(T_2)}{H_i(T_1)} \approx \exp\left[\frac{\overline{\Delta_{sol}H_i^{\infty}}}{R}\left(\frac{1}{T_2} - \frac{1}{T_1}\right)\right] \quad (15)$$

4. RESULTS AND DISCUSSION

4.1. Pure Ionic Liquid Thermal Conductivity. The measured thermal conductivity data for pure [EMIm][Tf_2N] over the range (298.15−398.15) K is reported in Table 4. The trends in thermal conductivity as a function of temperature are illustrated in Figure 1 alongside experimental data for pure [EMIm][Tf_2N] reported by Fröba et al.[59] and Ge et al.[57] as well as values predicted by Wu et al.[63] utilizing their group contribution method. The data reported in this study shows a percent decrease in thermal conductivity of 5% at 353.15 K relative to 298.15 K. A steeper decrease is observed at higher temperatures, as the percent decrease at 398.15 K relative to 298.15 K is approximately 20%. Moreover, the percent decrease in thermal conductivity at 398.15 K relative to that at 353.15 K is nearly 16%. We could find no literature data, in which to compare, above approximately 353.15 K. The percent average absolute relative deviations (%AARD) between the values measured in this work and those of Ge et al. and Fröba et al. (at corresponding temperatures) are 1.3% and 6.5%, respectively.

Figure 1 also illustrates the qualitative decrease in thermal conductivity with increasing temperature, as correlated by a modified Bridgman correlation[62] of the following form

$$\lambda = \Psi \rho^{(2/3)} MW^{(1/3)} c C_v \quad (16)$$

Table 4. Experimental Thermal Conductivity of Pure [EMIm][Tf_2N][a]

T (K)	λ (mW·m^{-1}·K^{-1})	λ/λ_o[b]
298.15	131.91	1.00
303.15	131.02	0.99
313.15	129.44	0.98
323.15	128.06	0.97
333.15	126.65	0.96
343.15	126.12	0.96
348.15	125.89	0.95
353.15	125.38	0.95
363.15	122.97	0.93
373.15	121.57	0.92
383.15	116.75	0.89
393.15	107.69	0.82
398.15	105.14	0.80

[a]Standard uncertainties: $u(T)$ = 0.1 K at (298.15−373.15) K and 0.2 K at (383.15−398.15) K; $u(\lambda)$ = 0.5 mW/m·K up to 323.15 K, 0.6 mW/m·K at (333.15−373.15) K, and 2.1 mW/m·K at (383.15−398.15) K. [b]λ/λ_o is the ratio of $\lambda(T)$ to $\lambda(T$ = 298.15 K).

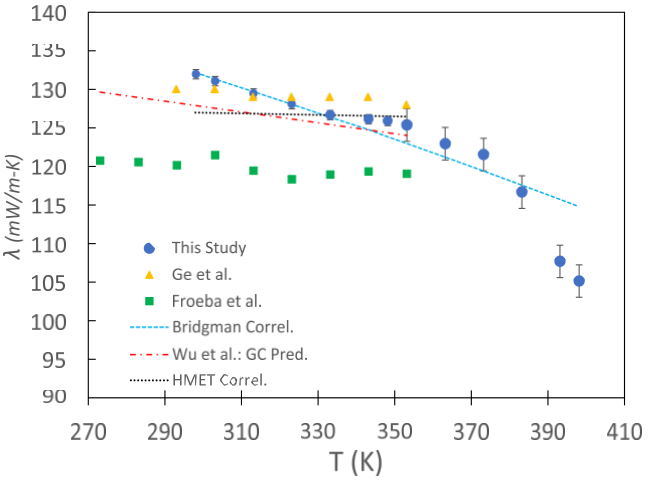

Figure 1. Thermal conductivity of pure [EMIm][Tf_2N] with temperature: (blue ●) this study; (yellow ▲) Ge et al.;[57] (green ■) Fröba et al.;[59] (blue dashed line) Bridgman correlation (eq 16); (black dotted line) HMET correlation (eq 17); (red dot-dashed line) Wu et al.[63]-group contribution prediction.

where ρ is the density (obtained from Tariq et al.[113]), MW is the molecular weight, c is the speed of sound (from Seoane et al.[114]), C_v is the isochoric heat capacity (estimated from data reported by Paulechka et al.[115]), and Ψ is a parameter regressed to the data with the objective function of the % AARD relative to the experimental values. The Bridgman equation regressed to our data ($\Psi = 8.333 \times 10^{-10}$) predicts a negative slope with temperature, as expected, and has a minimized %AARD of 3%. The density data, as reported in the literature, covers the entire temperature range of interest. However, the heat capacity data of Paulechka et al.[115] is only available to 370 K; hence, a linear extrapolation of the data was performed for the higher temperatures. The speed of sound data reported by Seoane et al.[114] were only available to 343.15 K and were linearly extrapolated throughout our entire temperature range. These linear extrapolations of speed of sound and heat capacity may or may not be quantitatively (or qualitatively) valid, which may account for the larger

https://doi.org/10.1021/acs.jced.2c00054
J. Chem. Eng. Data XXXX, XXX, XXX−XXX

Table 5. Parameters for the Pure Component Correlations Used in This Study[a]

	Ψ	Bridgman %AARD	A	B	HMET %AARD
[EMIm][Tf_2N][b]	8.333×10^{-10}	2.0%	3.1493	16.511	4.8%
[HMIm][Tf_2N][c]	8.234×10^{-10}	1.2%	−795.51	127.50	0.47%

[a]Ψ is the parameter of the Bridgman correlation (eq 16); *A* and *B* are parameters of the HMET correlation (eq 17). [b]See section 4.1 for applicable temperature ranges. [c]From ref 83. %AARD reported for each correlation with respect to measured values.

discrepancy between the model and our experimental data at the highest temperatures (see below).

The heuristic modification of the Enskog theory (HMET),[74] a two-parameter model, was utilized in an attempt to predict the trend in thermal conductivity with temperature and density. The HMET equation is reproduced below:

$$\lambda = A + B\ln(\rho) + 0.5\ln(T) \quad (17)$$

A and *B* are regressed parameters (values reported in Table 5), ρ is the density (obtained from Tariq et al.[113]), and *T* is the temperature in absolute Kelvin. The HMET model proved to be relatively reliable within the temperature range (298.15−353.15) K in which the %AARD is minimized to be ~1.5%. However, the model results become less accurate at higher temperatures in which the %AARD climbs to ~5%.

Figure 1 illustrates the general decrease in the thermal conductivity of pure [EMIm][Tf_2N] with temperature. The modified Bridgman equation exhibits increasing deviation from experimental values at higher temperatures; nevertheless, the Bridgman correlation has a maximum percent deviation of ~9%. The %AARD between the values predicted by the Bridgman correlation and experimental values is 0.7% for the temperature range (298.15−353.15) K and increases to 2% for the temperature range (298.15−398.15) K. The %AARD for the range (353.15−398.15) K is the highest among the data set (evaluating a minimum of five values) and is found to be 4%. The experimental data measured in this study can be modeled by a third-degree polynomial, as shown in eq 18

$$\lambda = -7.222 \times 10^{-5}(T)^3 + 7.243 \times 10^{-2}(T)^2 - 24.27(T) + 2.843 \times 10^{3} \quad (18)$$

in which *T* is the temperature in absolute Kelvin and within the range 298.15 K < *T* < 398.15 K. The %AARD between the values predicted by eq 18 and experimental data is 0.9% with a maximum deviation of 2 mW/m·K occurring at 383.15 K.

The results and analysis for the pure component [HMIm][Tf_2N] thermal conductivity have been described in detail in our previous work,[83] and a general overview of the pertinent results will be mentioned here. Similar to the trends in pure [EMIm][Tf_2N], the thermal conductivity of [HMIm][Tf_2N] decreases with increasing temperature (see Figure 1). The percent decrease in thermal conductivity from 293.15 K to 353.15 K is 4.3%. The pure [HMIm][Tf_2N] thermal conductivity values at (298.15, 323.15, 348.15) K are reported in Table 8 as the zero pressure data points. Both the modified Bridgman correlation (eq 16) and the HMET correlation (eq 17) well correlate the data for pure [HMIm][Tf_2N] (see Table 5).

4.2. Phase Behavior. The phase behavior of [HMIm][Tf_2N] and [EMIm][Tf_2N] with R-134a has been previously investigated by Ren et al.[84,104] Both systems are reported to have type V behavior as defined by the Scott−van Konynenburg scheme.[116] These systems exhibit a region of VLE at temperatures below the lower critical end point (LCEP) (335.75 K, 19 bar for [HMIm][Tf_2N] and 328.15 K, 15 bar for [EMIm][Tf_2N]) and below the vapor pressure of pure R-134a. At pressures at and above the saturation pressure, a one-phase miscible liquid region is attained. At temperatures above the LCEP and at approximately the vapor pressure of pure R-134a, VLLE exists until the upper critical end point (UCEP) which is approximately (within experimental accuracy) at the pure component critical point of R-134a (374.2 K, 40.6 bar). Between the LCEP and UCEP temperatures, VLE, VLLE, LLE, or mixture critical points (L = L and V = L) can exist depending on the pressure. The mixture critical point is attained only at relatively high pressures (reported above 100 bar for both ILs). At temperatures above the UCEP, VLE exists at all pressures below the mixture critical point.

In this study, the liquid thermal conductivity measurements were almost entirely measured in the vapor−liquid equilibrium regions. The isotherms at 298.15 K and 323.15 K fall below the LCEP of R-134a with both [EMIm][Tf_2N] and [HMIm][Tf_2N]. The isotherm at 348.15 K is between the LCEP and UCEP, and thus, vapor−liquid−liquid equilibrium, liquid−liquid equilibrium, and mixture critical points (L = L) are possible at and above the VLLE pressure (approximately the vapor pressure of pure R-134a). However, one LLE measurement was obtained. The measurement at 398.15 K is above the UCEP; thus, only VLE is possible until the mixture critical point (V = L) pressure.

4.3. [EMIm][Tf_2N] Solubility Modeling and Predictions. The mixture thermal conductivity was measured at a given temperature and pressure. To determine the composition of the equilibrium mixture, previously measured vapor−liquid equilibrium data were interpolated for the isotherms at 298.15 K and 348.15 K. However, no equilibrium data exists at 398.15 K. The Peng−Robinson equation of state (PR-EoS) coupled with the van der Waals one-parameter mixing rule was fit to the measured data (see Table 6 for k_{ij} parameters) and then used to predict at 398.15 K; see Figure 2. In addition, a Henry's constant method was utilized to model the known data and then extrapolate to 398.15 K.

Table 6. Mixing Rule Adjustable Parameters[a] and Model Performance for R-134a/[EMIm][Tf_2N] Fit to the Data of Ren et al.[104]

temperature (K)		%AARD
$k_{ij}^{(1)}$	0.101239641	
$k_{ij}^{(2)}$	−0.000313583	
298.15		11.6%
323.15		12.8%
348.15		14.7%

[a]$k_{ij} = k_{ij}^{(1)} + k_{ij}^{(2)}T$.

While the %AARD reported in Table 6 for the regressed values could be lowered by fitting at each isotherm or using a higher order equation than eq 10, the purpose was to

https://doi.org/10.1021/acs.jced.2c00054
J. Chem. Eng. Data XXXX, XXX, XXX−XXX

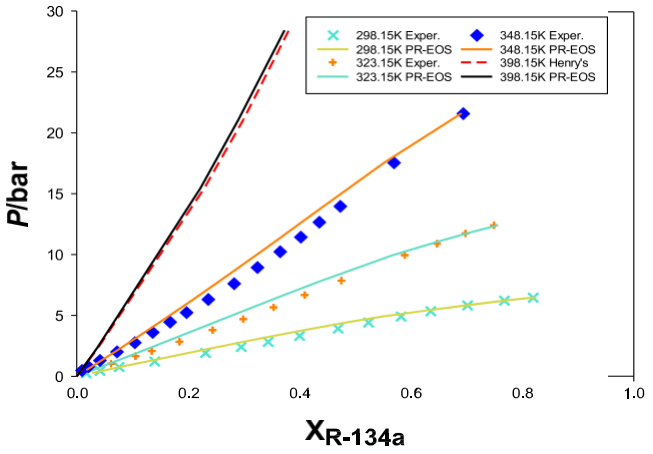

Figure 2. Experimental solubility data from ref 104 for [EMIm]-[Tf_2N] at 298.15 K (teal ×), 323.15 K (orange +), and 348.15 K (blue) compared to the Peng−Robinson EoS and vdW-1 predictions (solid lines). The solid black line corresponds to the Peng−Robinson and vdW-1 solubility prediction at 398.15 K, and the dashed red line corresponds to prediction of solubility at 398.15 K using a Henry's constant method as described in section 3.

extrapolate to the higher temperature. The maximum deviation in composition among the three isotherms is −0.0431 and occurs at T = 298.15 K and P = 3.35 bar. As illustrated in Figure 2, the PR-EoS and Henry's constant methods predict similar solubility results at 398.15 K. The average absolute relative deviation between the values predicted by the two methods at 398.15 K is 0.006 with an average percent difference of 2.88%. The calculated Henry's constants are reported in Table S1. Thus, we believe that the predicted compositions at 398.15 K are within ∼5% on average. However, it should be further noted that these are extrapolation values and would need further experimental measurements to completely verify.

4.4. R-134a-Saturated [EMIm][Tf_2N] Thermal Conductivity. The thermal conductivity of the [EMIm][Tf_2N] and R-134a system was measured at (298.15, 348.15, 398.15) K and various pressures, mostly in the VLE regime, and shown in Figure 3. A general decrease in thermal conductivity is

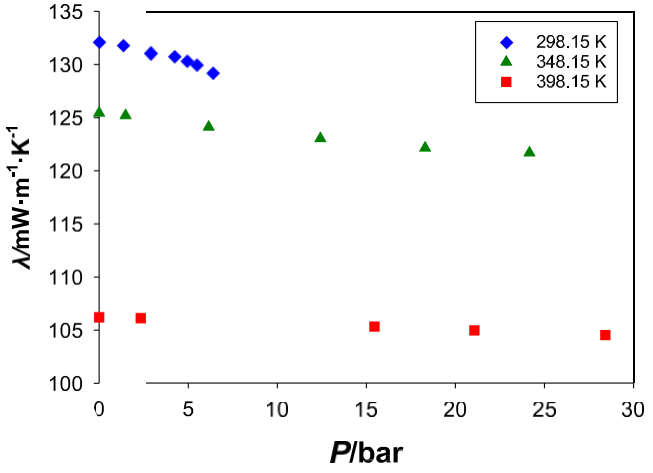

Figure 3. Thermal conductivity of R-134a-saturated [EMIm][Tf_2N] with pressure and at three isotherms: (blue ♦) 298.15 K; (green ▲) 348.15 K; (red ■) 398.15 K.

observed at all three isotherms with increasing pressure of R-134a. Throughout all of the isotherms and at all pressures investigated, the maximum percent decrease is only 3%. The decrease at all three isotherms with pressure is relatively linear at the lower pressures.

Solubility data and EoS predictions as detailed above were used to correlate the molar compositions of R-134a in the mixture at the temperature and pressure of the thermal conductivity experiments. Experimental solubility data were interpolated at 298.15 K and 348.15 K; interpolated values are believed to be accurate to ∼3%. Molar compositions at 398.15 K were predicted using the EoS; the accuracy of those values is not readily assessed, as no experimental data exists at this temperature. It is believed to be about ∼5%, but future experimental confirmation may be needed for more precise engineering purposes. Pressure, composition, and thermal conductivity values are reported in Table 7.

Table 7. Thermal Conductivity, Pressure, and Molar Composition of R-134a-Saturated [EMIm][Tf_2N][a]

T/K	P/bar	$x_{R\text{-}134a}$	λ/mW·m^{-1}·K^{-1}	λ/λ_0
298.15[b]	0.0[d]	0.00	132.13	1.000
	1.34	0.15	131.82	0.998
	2.87	0.34	131.09	0.992
	4.22	0.50	130.76	0.990
	4.92	0.59	130.33	0.986
	5.46	0.66	129.98	0.984
	6.35	0.79	129.23	0.978
	6.56	0.91	100.45	0.760
348.15[b]	0.00[d]	0.00	125.44	1.000
	1.48	0.05	125.21	0.998
	6.15	0.22	124.12	0.989
	12.42	0.43	123.04	0.981
	18.3	0.60	122.15	0.974
	24.16[e]	0.74	121.69	0.970
398.15[c]	0.0[d]	0.00	106.20	1.000
	2.33	0.04	106.12	0.999
	15.5	0.22	105.31	0.992
	21.1	0.29	104.96	0.988
	28.4	0.37	104.51	0.984

[a]Reported standard uncertainties: $u(T)$ = 0.1 K; $u(P)$ = 0.1 bar; $u(\lambda)$ = 2.2 mW/m·K (reported as the highest uncertainty of all measurements; section 2.2); $u(x)$ = 0.04 (reported as the highest uncertainty of all data points; section 2.2). [b]Compositions interpolated/extrapolated from the data of Ren and Scurto.[104] [c]Compositions predicted using EoS. [d]Pure IL at ambient pressure (gauge). [e]In liquid−liquid equilibrium (LLE).

Figure 4 illustrates the decrease in thermal conductivity with increasing R-134a compositions. The trend of decreasing thermal conductivity with increasing R-134a composition is observed at all three isotherms, with the steepest decrease occurring at the isotherm of 348.15 K. It should be noted that even at 80% mol of R-134a in the mixture, the thermal conductivity of the liquid phase only decreases by ∼3%. This is quite surprising given that the thermal conductivity of R-134a is much lower than the IL's. The thermal conductivity of pure saturated liquid R-134a is 81.134 mW/m·K at 298.15 K, 70.427 mW/m·K at 323.15 K, and 59.421 mW/m·K at 348.15 K.[78,93] This is significantly lower than the pure IL or even the IL mixture to the maximum measured composition of ∼80% mol R-134a.

https://doi.org/10.1021/acs.jced.2c00054
J. Chem. Eng. Data XXXX, XXX, XXX−XXX

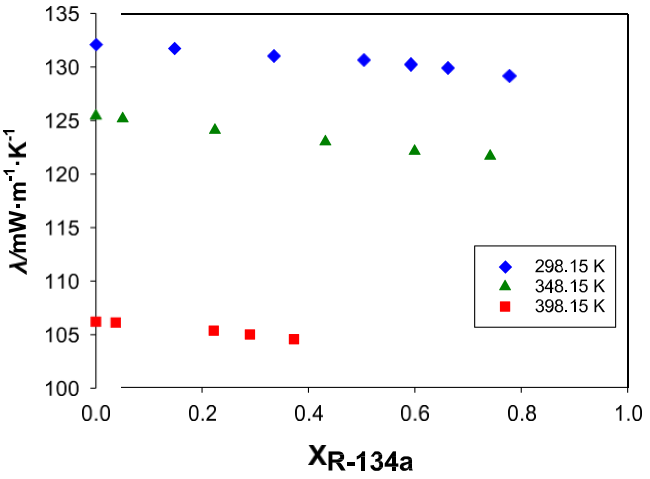

Figure 4. Thermal conductivity of R-134a-saturated [EMIm][Tf_2N] with compositions and at three isotherms: (blue ♦) 298.15 K; (green ▲) 348.15 K; (red ■) 398.15 K.

How does the IL/R-134a mixture transition at very high compositions of R-134a to connect to these lower pure saturated liquid values? An additional measurement was conducted at a composition of R-134a of ~90% mol. These measurements are more challenging due to the large volume expansion of sometimes 300+% with 80+% R-134a. Figure 5

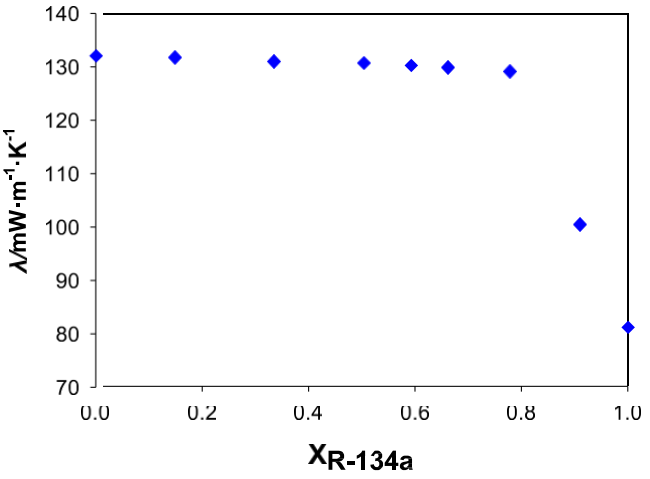

Figure 5. (blue ♦) Thermal conductivity of R-134a-saturated [EMIm][Tf_2N] and pure, saturated liquid R-134a at 298.15 K. Saturated liquid R-134a thermal conductivity value obtained from refs 78 and 93.

illustrates that, at very high compositions of R-134a, the mixture thermal conductivity exhibits a more pronounced decrease. Thus, the heat transfer mechanism for the IL remains relatively constant until compositions of R-134a reach between 80 and 90% mol of R-134a. An important ramification of this behavior is that simple mixing rules using composition and the pure components' thermal conductivity would be inappropriate both qualitatively and quantitatively. Thus, actual mixture data is required, and a better understanding of the mixture structure is needed to develop more accurate models for both regression and prediction.

4.5. R-134a-Saturated [HMIm][Tf_2N] Thermal Conductivity. The thermal conductivity for the R-134a-saturated [HMIm][Tf_2N] system was measured at (298.15, 323.15, 348.15) K and various pressures in a similar manner as done for the R-134a-saturated [EMIm][Tf_2N] system. The measured data for [HMIm][Tf_2N]/R-134a shows a linear decrease in thermal conductivity over the pressure ranges investigated in this study. All measurements for this system have been conducted in the VLE regime. The greatest decrease is observed at 348.15 K and a pressure of 18.84 bar in which the percent decrease is ~9%. The trends of increasing thermal conductivity with increasing pressure (induced with introduction of R-134a) are illustrated in Table 8. Solubility data

Table 8. Thermal Conductivity, Pressure, and Molar Composition of R-134a-Saturated [HMIm][Tf_2N][a]

T/K	P/bar	$x_{R\text{-}134a}$	λ/mW·m^{-1}·K^{-1}	λ/λ_0
298.15[b]	0.0[c]	0.00	128.43	1.000
	1.00	0.12	127.67	0.994
	1.49	0.19	127.34	0.992
	1.98	0.26	126.96	0.989
	2.54	0.33	126.45	0.985
	3.86	0.51	126.17	0.982
	5.34	0.69	125.47	0.977
323.15[b]	0.0[c]	0.00	125.44	1.000
	1.32	0.10	124.65	0.997
	2.63	0.19	124.01	0.992
	3.97	0.29	123.21	0.986
	5.28	0.37	122.18	0.977
	7.81	0.52	119.12	0.953
	10.55	0.68	116.61	0.933
348.15[b]	0.0[c]	0.00	123.75	1.000
	2.28	0.12	120.60	0.975
	4.66	0.23	119.74	0.968
	9.52	0.42	116.43	0.941
	14.8	0.59	114.38	0.924
	18.84	0.73	113.20	0.915

[a]Reported standard uncertainties: $u(T)$ = 0.1 K; $u(P)$ = 0.1 bar; $u(\lambda)$ = 0.5 mW/m·K at 298.15 K and 323.15 K and $u(\lambda)$ = 0.6 mW/m·K at 348.15 K; $u(x)$ = 0.02. [b]Compositions, interpolated/extrapolated from the data of Ren and Scurto.[85] [c]Pure IL at ambient pressure (gauge) reported in previous work.[83]

reported by Ren and Scurto[85] were used to correlate the pressure to molar composition of R-134a in the mixture within the VLE regions investigated. Solubility values interpolated for the pressures of interest are estimated to be accurate to 3%. Pressure, molar compositions of R-134a, and thermal conductivity of the R-134a-saturated [HMIm][Tf_2N] system are reported in Table 8. The trends in thermal conductivity with increasing R-134a composition are illustrated in Figure 6. Figure 6 illustrates the decrease in thermal conductivity with increasing molar composition of R-134a in [HMIm][Tf_2N]. The steepest decrease occurs at 348.15 K; the percent decrease at 348.15 K and a R-134a molar composition of 0.73 is 8% relative to the pure IL thermal conductivity at the same temperature. The percent decrease at 323.15 K and a R-134a molar composition of 0.68 is 7%. The shallowest decrease is observed at 298.15 K, in which, at a molar composition of 0.69, the decrease relative to the pure IL thermal conductivity is merely 2.3%.

4.6. Analysis of Phenomena. In both cases, R-134a-saturated [EMIm][Tf_2N] and R-134a-saturated [HMIm]-[Tf_2N], a general decrease in thermal conductivity with increasing molar compositions of R-134a is observed. This

https://doi.org/10.1021/acs.jced.2c00054
J. Chem. Eng. Data XXXX, XXX, XXX−XXX

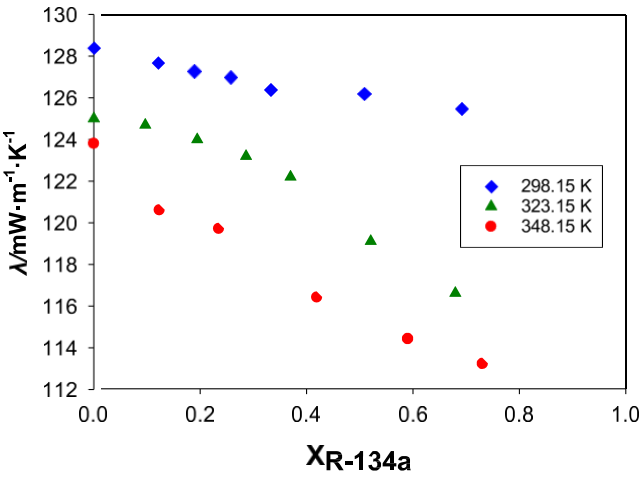

Figure 6. Thermal conductivity of R-134a-saturated [HMIm][Tf_2N] with composition and at three isotherms: (blue ♦) 298.15 K; (green ▲) 323.15 K; (red ●) 348.15 K.

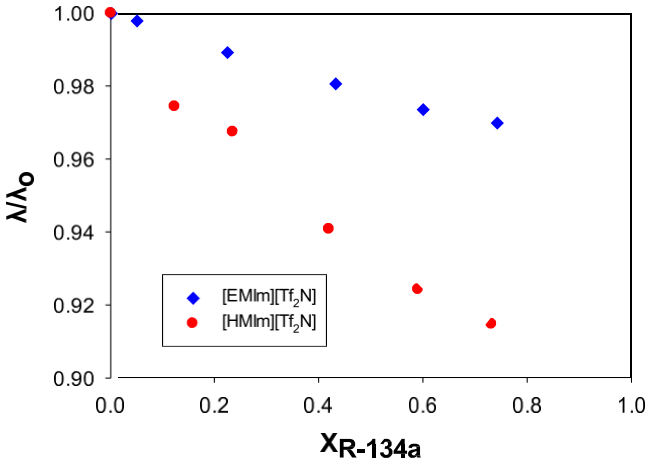

Figure 7. Change in the relative thermal conductivity of R-134a-saturated [EMIm][Tf_2N] (blue ♦) and R-134a-saturated [HMIm]-[Tf_2N] (red ●) at 348.15 K and various compositions.

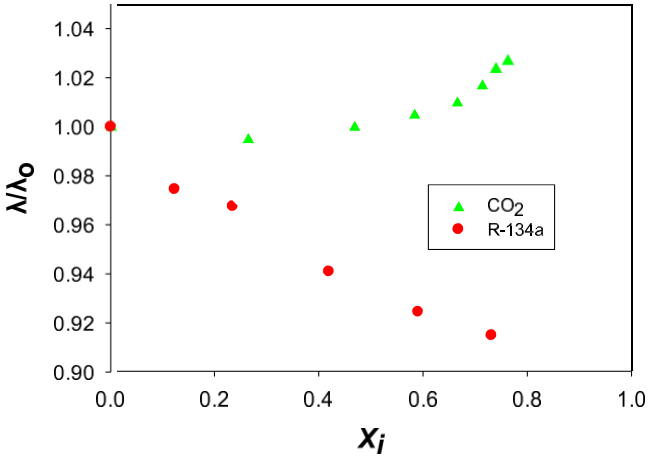

Figure 8. Change in relative thermal conductivity of R-134a-saturated [HMIm][Tf_2N] (red ●) and CO_2-saturated [HMIm][Tf_2N] (green ▲) at 348.15 K[83] and various molar compositions of each respective gas (*i*).

decrease is attributed to a diluent effect in which a component with a lower thermal conductivity, R-134a, is added to one with a higher thermal conductivity, the IL. However, in both cases, the thermal conductivity of the mixture remains close to that of the pure IL thermal conductivity at the same temperature and ambient pressure. That is, the mixture's thermal conductivity at low to moderate R-134a compositions is dominated by that of the pure IL's thermal conductivity and is not an equal contribution of both components. Hence, linear mixing rules based on the weighted average composition of each component would not be applicable across the composition range in predicting the thermal conductivity of the mixture. Such mixing rules may result in underpredictions in thermal conductivity of up to ~30%. A more detailed analysis of the applicability of simple mixing rules in estimating the thermal conductivity of IL/gas mixtures is presented in our previous work.[83] This behavior is in stark contrast with our measurements of the dynamic viscosity of the R-134a and ILs previously measured[55] which demonstrated up to 80+% decreases in viscosity with moderate compositions of the low-viscosity R-134a. Comparison of these viscosity measurements and thermal conductivity measurements clearly shows a large diluent effect for momentum transport properties but does not lead to similar effects for heat transport properties.

Figure 7 illustrates the decrease in relative thermal conductivity in the [EMIm][Tf_2N]/R-134a system compared to that of the [HMIm][Tf_2N]/R-134a system with increasing molar composition of R-134a at 348.15 K. Relative thermal conductivity is the thermal conductivity of the mixture divided by the pure IL thermal conductivity at the same temperature. This allows direct comparison of the composition effect of two ILs which have different pure component thermal conductivities. As shown, a steeper decrease is observed in the case of the IL with the longer alkyl group on the cation. This trend is also observed at 298.15 K. The longer alkyl chain on the imidazolium seems to experience a larger diluent effect at a given composition of R-134a.

We have previously investigated the thermal conductivity of CO_2-saturated [HMIm][Tf_2N].[83] Figure 8 illustrates the difference in thermal conductivity behavior between the relative thermal conductivity for the IL saturated with CO_2 versus R-134a. Initially, there is a slight linear decrease in the liquid thermal conductivity with an increase in both R-134a and CO_2 composition. However, while the thermal conductivity of the IL saturated with R-134a continues to decrease with increasing compositions, the thermal conductivity with CO_2 actually passes through a minimum and then seemingly increases with composition. The different behavior is attributed mainly to the pressures needed to achieve the same composition. For instance, at 348.15 K, a 70% mol solubility of CO_2 is attained at a pressure of ~140 bar, whereas, in the R-134a case, a 70% mol composition is attained at a pressure of ~18 bar. The effect of hydrostatic pressure on the thermal conductivity of pure [HMIm][Tf_2N] was previously measured and indicates an increase in the thermal conductivity with pressure over the ~180 bar range that the mixture data was measured.[83] Thus, for the CO_2/IL mixture data, the increase in thermal conductivity at higher CO_2 composition is where hydrostatic effects dominate diluent/composition effects. R-134a is more readily soluble at lower pressures than CO_2; hence, hydrostatic pressure effects never outweigh diluent effects across the pressure ranges investigated.

The mechanism of solubility of both R-134a and CO_2 in the ionic liquid is mostly attributed to the free volume available for

https://doi.org/10.1021/acs.jced.2c00054
J. Chem. Eng. Data XXXX, XXX, XXX−XXX

the gas to occupy.[83,117−121] While the presence of either of the dissolved gases does slightly decrease the thermal conductivity (in the lower pressure range for CO_2) within the IL, neither gas is capable of significantly changing the mechanism of heat transport found within the IL itself. To significantly change the heat transport mechanism, some higher level of solvation is believed to be required. The dielectric constant of CO_2 is very low ($\varepsilon \sim 1.41$ for saturated liquid CO_2 at 299 K)[122] and not likely able to solvate the ions to any appreciable extent. While R-134a is more polar than CO_2 ($\varepsilon = 9.24$ as a saturated liquid at 298.15 K),[123] it still is not polar enough to fully solvate the IL or the cations and anions. This is contrasted with the behavior reported by Chen et al. for the thermal conductivity of the IL, 1-ethyl-3-methylimidazolium ethylsulfate ([EMIm][$EtSO_4$]), and water mixtures at ambient pressure.[124] Here, the thermal conductivity of the IL/water mixture exhibits a relatively linear change with composition connecting the pure component thermal conductivities. The dielectric constant of water at 298.15 K is 78.4.[93] Hence, it is expected that the IL mixtures dissociate into fully solvated ions at moderate compositions of water. Further studies on the nature of solubility of the different compounds in the ILs are needed to better assess the effects on the thermal properties of the mixture.

5. CONCLUSIONS

Proper knowledge of the thermal properties of pure ionic liquids as well as mixtures of ionic liquids saturated with gases is imperative for optimal design of various systems. This study reports on the thermal conductivities of the ILs [EMIm][Tf_2N] and [HMIm][Tf_2N] saturated with R-134a. The thermal conductivity of the pure ILs decreases with increasing temperature. Increasing the molar composition of R-134a decreases the thermal conductivity of the mixture in both systems. However, the thermal conductivity of the mixture continues to be dominated by that of the IL at low to moderate molar compositions of R-134a. A drastic decrease in the thermal conductivity of the mixture is not observed until very high molar compositions of R-134a are attained (~90% mol). It is believed that the dominant mechanism of gas dissolution is the filling of the free volume within the structure of the IL; hence, the low-polarity gas does not fully solvate the IL or drastically alter its structure or heat transport mechanism. Solubility of R-134a in both ILs occurs over a relatively low-pressure regime, and only a diluent effect is observed without significant hydrostatic effects. Simple mixing rules based on the compositions of the components in the mixture and their pure component thermal conductivities are not qualitatively nor quantitatively correct. The IL with the longer alkyl-chain length on the cation, [HMIm][Tf_2N], exhibits a steeper decrease in thermal conductivity with increasing molar compositions of R-134a. Further investigation of solubility mechanisms and the chemical nature of solute interactions is needed to better assess the effects on the thermal properties of ionic liquids and dissolved gas systems.

ASSOCIATED CONTENT

Supporting Information

The Supporting Information is available free of charge at https://pubs.acs.org/doi/10.1021/acs.jced.2c00054.

^{1}H NMR spectra for [HMIm][Tf_2N] and [EMIm][Tf_2N]; calculated Henry's constants with standard uncertainties associated with their respective linear fit for R-134a-saturated [EMIm][Tf_2N] at the three isotherms with available solubility data as well as the predicted Henry's constant at 398.15 K; the calculated partial molar enthalpy of solution and partial molar entropy of solution; and plot of the thermal conductivity of [HMIm][Tf_2N] at the three isotherms measured as a function of pressure (PDF)

AUTHOR INFORMATION

Corresponding Author

Aaron M. Scurto − *Department of Chemical & Petroleum Engineering, University of Kansas, Lawrence, Kansas 66045, United States; Center for Environmentally Beneficial Catalysis, University of Kansas, Lawrence, Kansas 66047, United States;* orcid.org/0000-0001-7214-1871; Phone: (785) 864-4947; Email: ascurto@ku.edu; Fax: (785) 864-4967

Author

Karim S. Al-Barghouti − *Department of Chemical & Petroleum Engineering, University of Kansas, Lawrence, Kansas 66045, United States; Center for Environmentally Beneficial Catalysis, University of Kansas, Lawrence, Kansas 66047, United States*

Complete contact information is available at: https://pubs.acs.org/10.1021/acs.jced.2c00054

Notes

The authors declare no competing financial interest.

ACKNOWLEDGMENTS

We would like to thank the US National Science Foundations (NSF) for financial support under grants EEC-1852308 and EFRI-2029354.

REFERENCES

(1) Van Rantwijk, F.; Sheldon, R. A. Biocatalysis in Ionic Liquids. *Chem. Rev.* 2007, *107* (6), 2757−2785.

(2) Hough, W. L.; Smiglak, M.; Rodriguez, H.; Swatloski, R. P.; Spear, S. K.; Daly, D. T.; Pernak, J.; Grisel, J. E.; Carliss, R. D.; Soutullo, M. D.; Davis, J. H., Jr.; Rogers, R. D. The third evolution of ionic liquids: active pharmaceutical ingredients. *New J. Chem.* 2007, *31* (8), 1429.

(3) Steinrück, H.-P.; Wasserscheid, P. Ionic Liquids in Catalysis. *Catal. Lett.* 2015, *145* (1), 380−397.

(4) Ahosseini, A.; Ren, W.; Scurto, A. M. Homogeneous catalysis in biphasic ionic liquid/CO_2 systems. *Chim Oggi* 2007, *25* (2), 40−42.

(5) McNeice, P.; Marr, P. C.; Marr, A. C. Basic ionic liquids for catalysis: the road to greater stability. *Catal. Sci. Technol.* 2021, *11* (3), 726−741.

(6) Elhenawy, S.; Khraisheh, M.; Almomani, F.; Hassan, M. Key Applications and Potential Limitations of Ionic Liquid Membranes in the Gas Separation Process of CO2, CH4, N2, H2 or Mixtures of These Gases from Various Gas Streams. *Molecules* 2020, *25* (18), 4274.

(7) Afzal, W.; Liu, X.; Prausnitz, J. M. Physical data for a process to separate krypton from air by selective absorption in an ionic liquid. *Fluid Phase Equilib.* 2015, *404*, 124−130.

(8) Shiflett, M. B.; Niehaus, A. M. S.; Yokozeki, A. Separation of N_2O and CO_2 Using Room-Temperature Ionic Liquid [bmim][BF_4]. *J. Phys. Chem. B* 2011, *115* (13), 3478−3487.

(9) Shiflett, M. B.; Yokozeki, A. Separation of Carbon Dioxide and Sulfur Dioxide Using Room-Temperature Ionic Liquid [bmim][$MeSO_4$]. *Energy Fuels* 2010, *24* (2), 1001−1008.

(10) Shiflett, M. B.; Yokozeki, A. Separation of CO_2 and H_2S using room-temperature ionic liquid [bmim][PF_6]. *Fluid Phase Equilib.* 2010, *294* (1−2), 105−113.
(11) Shiflett, M. B.; Yokozeki, A. Chemical Absorption of Sulfur Dioxide in Room-Temperature Ionic Liquids. *Ind. Eng. Chem. Res.* 2010, *49* (3), 1370−1377.
(12) Yokozeki, A.; Shiflett, M. B. Separation of Carbon Dioxide and Sulfur Dioxide Gases Using Room-Temperature Ionic Liquid [hmim][Tf_2N]. *Energy Fuels* 2009, *23* (9), 4701−4708.
(13) Asensio-Delgado, S.; Pardo, F.; Zarca, G.; Urtiaga, A. Absorption separation of fluorinated refrigerant gases with ionic liquids: Equilibrium, mass transport, and process design. *Sep. Purif. Technol.* 2021, *276*, 119363.
(14) Sosa, J. E.; Ribeiro, R. P. P. L.; Castro, P. J.; Mota, J. P. B.; Araújo, J. M. M.; Pereiro, A. B. Absorption of Fluorinated Greenhouse Gases Using Fluorinated Ionic Liquids. *Ind. Eng. Chem. Res.* 2019, *58* (45), 20769−20778.
(15) Pardo, F.; Gutiérrez-Hernández, S. V.; Hermida-Merino, C.; Araújo, J. M. M.; Piñeiro, M. M.; Pereiro, A. B.; Zarca, G.; Urtiaga, A. Integration of Stable Ionic Liquid-Based Nanofluids into Polymer Membranes. Part II: Gas Separation Properties toward Fluorinated Greenhouse Gases. *Nanomaterials* 2021, *11* (3), 582.
(16) Asensio-Delgado, S.; Jovell, D.; Zarca, G.; Urtiaga, A.; Llovell, F. Thermodynamic and process modeling of the recovery of R410A compounds with ionic liquids. *Int. J. Refrig.* 2020, *118*, 365−375.
(17) Watanabe, M.; Thomas, M. L.; Zhang, S.; Ueno, K.; Yasuda, T.; Dokko, K. Application of Ionic Liquids to Energy Storage and Conversion Materials and Devices. *Chem. Rev.* 2017, *117* (10), 7190−7239.
(18) Bakonyi, P.; Koók, L.; Rózsenberszki, T.; Tóth, G.; Bélafi-Bakó, K.; Nemestóthy, N. Development and Application of Supported Ionic Liquid Membranes in Microbial Fuel Cell Technology: A Concise Overview. *Membranes* 2020, *10* (1), 16.
(19) Díaz, M.; Ortiz, A.; Ortiz, I. Progress in the use of ionic liquids as electrolyte membranes in fuel cells. *J. Membr. Sci.* 2014, *469*, 379−396.
(20) Hou, H.; Schütz, H. M.; Giffin, J.; Wippermann, K.; Gao, X.; Mariani, A.; Passerini, S.; Korte, C. Acidic Ionic Liquids Enabling Intermediate Temperature Operation Fuel Cells. *ACS Appl. Mater. Interfaces* 2021, *13* (7), 8370−8382.
(21) Qi, H.; Ren, Y.; Guo, S.; Wang, Y.; Li, S.; Hu, Y.; Yan, F. High-Voltage Resistant Ionic Liquids for Lithium-Ion Batteries. *ACS Appl. Mater. Interface* 2020, *12* (1), 591−600.
(22) Boesmann, A.; Schubert, T. Absorption Refrigeration Machines and Heat Transformers. WIPO 2005113702A1, 2005.
(23) Shiflett, M. B.; Yokozeki, A. Absorption Cycle Utilizing Ionic Liquid as Working Fluid. WO2006084262A1, 2006.
(24) Moreno, D.; Ferro, V. R.; De Riva, J.; Santiago, R.; Moya, C.; Larriba, M.; Palomar, J. Absorption refrigeration cycles based on ionic liquids: Refrigerant/absorbent selection by thermodynamic and process analysis. *Appl. Energ* 2018, *213*, 179−194.
(25) Esaki, T.; Kobayashi, N.; Uchiyama, H.; Matsukuma, Y. Characteristics of Absorption Equilibrium with HFC-134a and an Ionic Liquid Pair. *J. Mater. Sci. Chem. Eng.* 2019, *07* (03), 65−78.
(26) Ren, W. High-Pressure Phase Equilibria of Ionic Liquids and Compressed Gases for Applications in Reactions and Absorption Refrigeration. Ph.D. Dissertation, University of Kansas, 2009.
(27) Kim, Y. J.; Gonzalez, M. Exergy analysis of an ionic-liquid absorption refrigeration system utilizing waste-heat from datacenters. *Int. J. Refrig.* 2014, *48*, 26−37.
(28) Kim, Y. J.; Kim, S.; Joshi, Y. K.; Fedorov, A. G.; Kohl, P. A. Thermodynamic analysis of an absorption refrigeration system with ionic-liquid/refrigerant mixture as a working fluid. *Energy* 2012, *44* (1), 1005−1016.
(29) Liu, X.; Pan, P.; He, M. Vapor-liquid equilibrium and diffusion coefficients of R32 + [HMIM][FEP], R152a + [HMIM][FEP] and R161 + [HMIM][FEP]. *J. Mol. Liq.* 2018, *253*, 28−35.
(30) Khamooshi, M.; Parham, K.; Atikol, U. Overview of Ionic Liquids Used as Working Fluids in Absorption Cycles. *Adv. Mech. Eng.* 2013, *5*, 620592.
(31) Shukla, S. K.; Khokarale, S. G.; Bui, T. Q.; Mikkola, J.-P. T. Ionic Liquids: Potential Materials for Carbon Dioxide Capture and Utilization. *Front. Mater.* 2019, *6*, No. 42.
(32) Aghaie, M.; Rezaei, N.; Zendehboudi, S. A systematic review on CO_2 capture with ionic liquids: Current status and future prospects. *Renew. Sust. Energy Rev.* 2018, *96*, 502−525.
(33) Mesbah, M.; Pouresmaeil, S.; Galledari, S. A.; Momeni, M.; Shahsavari, S.; Soroush, E. Ionic Liquids for Carbon Dioxide Capture. *Sustainable Agriculture Reviews*, Vol. *38*; Springer: Cham, Switzerland, 2020; pp 121−148.
(34) Asensio-Delgado, S.; Pardo, F.; Zarca, G.; Urtiaga, A. Enhanced absorption separation of hydrofluorocarbon/hydrofluoroolefin refrigerant blends using ionic liquids. *Sep. Purif. Technol.* 2020, *249*, 117136.
(35) Sun, Y.; Zhang, Y.; Wang, X.; Prausnitz, J. M.; Jin, L. Gaseous absorption of 2,3,3,3-tetrafluoroprop-1-ene in three imidazolium-based ionic liquids. *Fluid Phase Equilib.* 2017, *450*, 65−74.
(36) Zarca, G.; Ortiz, I.; Urtiaga, A. Recovery of carbon monoxide from flue gases by reactive absorption in ionic liquid imidazolium chlorocuprate(I): Mass transfer coefficients. *Chin. J. Chem. Eng.* 2015, *23* (5), 769−774.
(37) Albà, C. G.; Vega, L. F.; Llovell, F. Assessment on Separating Hydrofluoroolefins from Hydrofluorocarbons at the Azeotropic Mixture R513A by Using Fluorinated Ionic Liquids: A Soft-SAFT Study. *Ind. Eng. Chem. Res.* 2020, *59* (29), 13315−13324.
(38) Lepre, L. F.; Andre, D.; Denis-Quanquin, S.; Gautier, A.; Padua, A. A. H.; Costa Gomes, M. Ionic Liquids Can Enable the Recycling of Fluorinated Greenhouse Gases. *ACS Sus. Chem. Eng.* 2019, *7* (19), 16900−16906.
(39) Sosa, J. E.; Santiago, R.; Hospital-Benito, D.; Costa Gomes, M.; Araújo, J. M. M.; Pereiro, A. B.; Palomar, J. Process Evaluation of Fluorinated Ionic Liquids as F-Gas Absorbents. *Environ. Sci. Technol.* 2020, *54* (19), 12784−12794.
(40) Castro, P. J.; Redondo, A. E.; Sosa, J. E.; Zakrzewska, M. E.; Nunes, A. V. M.; Araújo, J. M. M.; Pereiro, A. B. Absorption of Fluorinated Greenhouse Gases in Deep Eutectic Solvents. *Ind. Eng. Chem. Res.* 2020, *59* (29), 13246−13259.
(41) Baca, K. R.; Olsen, G. M.; Matamoros Valenciano, L.; Bennett, M. G.; Haggard, D. M.; Befort, B. J.; Garciadiego, A.; Dowling, A. W.; Maginn, E. J.; Shiflett, M. B. Phase Equilibria and Diffusivities of HFC-32 and HFC-125 in Ionic Liquids for the Separation of R-410A. *ACS Sus. Chem. Eng.* 2022, *10*, 816.
(42) United States Environmental Protection Agency. Overview of Greenhouse Gases. https://www.epa.gov/ghgemissions/overview-greenhouse-gases (accessed 2021).
(43) Graziosi, F.; Arduini, J.; Furlani, F.; Giostra, U.; Cristofanelli, P.; Fang, X.; Hermanssen, O.; Lunder, C.; Maenhout, G.; O'Doherty, S.; Reimann, S.; Schmidbauer, N.; Vollmer, M.K.; Young, D.; Maione, M. European emissions of the powerful greenhouse gases hydrofluorocarbons inferred from atmospheric measurements and their comparison with annual national reports to UNFCCC. *Atmos. Environ.* 2017, *158*, 85−97.
(44) Ebnesajjad, S. *Concise Handbook of Fluorocarbon Gases: Applications in Refrigeration and Other Industries*; Wiley: 2021.
(45) McLinden, M. O.; Huber, M. L. (R)Evolution of Refrigerants. *J. Chem. Eng. Data* 2020, *65* (9), 4176−4193.
(46) EPA. Recent International Developments under the Montreal Protocol; 2016; https://www.epa.gov/ozone-layer-protection/recent-international-developments-under-montreal-protocol (accessed 2021).
(47) Booten, C.; Nicholson, S.; Mann, M.; Abdelaziz, O. *Refrigerants: Market Trends and Supply Chain Assessment*; Office of Scientific and Technical Information (OSTI): 2020. DOI: 10.2172/1599577.
(48) EPA. Significant New Alternatives Policy. In *EPA-HQ-OAR-2013-0748; FRL-9922-26-OAR*; 2015.

https://doi.org/10.1021/acs.jced.2c00054
J. Chem. Eng. Data XXXX, XXX, XXX−XXX

(49) Mota-Babiloni, A.; Navarro-Esbrí, J.; Makhnatch, P.; Molés, F. Refrigerant R32 as lower GWP working fluid in residential air conditioning systems in Europe and the USA. *Renew. Sust. Energy Rev.* 2017, *80*, 1031−1042.
(50) Morais, A. R. C.; Harders, A. N.; Baca, K. R.; Olsen, G. M.; Befort, B. J.; Dowling, A. W.; Maginn, E. J.; Shiflett, M. B. Phase Equilibria, Diffusivities, and Equation of State Modeling of HFC-32 and HFC-125 in Imidazolium-Based Ionic Liquids for the Separation of R-410A. *Ind. Eng. Chem. Res.* 2020, *59* (40), 18222−18235.
(51) Shiflett, M. B.; Yokozeki, A. Utilizing ionic liquids for hydrofluorocarbon separation. US Patent US8,628,644B2, 2006.
(52) Shiflett, M. B.; Corbin, D. R.; Elliott, B. A.; Yokozeki, A. Sorption of trifluoromethane in zeolites and ionic liquid. *J. Chem. Thermodyn.* 2013, *64*, 40−49.
(53) Shiflett, M. B.; Shiflett, A. D.; Yokozeki, A. Separation of tetrafluoroethylene and carbon dioxide using ionic liquids. *Sep. Purif. Technol.* 2011, *79* (3), 357−364.
(54) Shiflett, M. B.; Yokozeki, A. Process for purifying perfluorinated products. US Patent US8,771,626B2, 2007.
(55) Ahosseini, A.; Ren, W.; Weatherley, L. R.; Scurto, A. M. Viscosity and self-diffusivity of ionic liquids with compressed hydrofluorocarbons: 1-Hexy1−3-methyl-imidazolium bis-(trifluorosulfonyl)amide and 1,1,1,2-tetrafluoroethane. *Fluid Phase Equilib.* 2017, *437*, 34−42.
(56) Al-Barghouti, K. S.; Baca, K. R.; Shiflett, M. B.; Scurto, A. M. Thermodynamic and Transport Properties of the Ionic Liquid 1-ethyl-3-methylimidazolium bis(trifluoromethylsulfonyl)amide and Compressed Pentafluoroethane and Difluoromethane. Manuscript in progress, 2022.
(57) Ge, R.; Hardacre, C.; Nancarrow, P.; Rooney, D. W. Thermal conductivities of ionic liquids over the temperature range from 293 to 353 K. *J. Chem. Eng. Data* 2007, *52* (5), 1819−1823.
(58) Frez, C.; Diebold, G. J.; Tran, C. D.; Yu, S. Determination of thermal diffusivities, thermal conductivities, and sound speeds of room-temperature ionic liquids by the transient grating technique. *J. Chem. Eng. Data* 2006, *51* (4), 1250−1255.
(59) Fröba, A. P.; Rausch, M. H.; Krzeminski, K.; Assenbaum, D.; Wasserscheid, P.; Leipertz, A. Thermal Conductivity of Ionic Liquids: Measurement and Prediction. *Int. J. Thermophys* 2010, *31* (11−12), 2059−2077.
(60) Liu, H.; Maginn, E.; Visser, A. E.; Bridges, N. J.; Fox, E. B. Thermal and Transport Properties of Six Ionic Liquids: An Experimental and Molecular Dynamics Study. *Ind. Eng. Chem. Res.* 2012, *51* (21), 7242−7254.
(61) Chen, Q. L.; Wu, K. J.; He, C. H. Thermal Conductivity of Ionic Liquids at Atmospheric Pressure: Database, Analysis, and Prediction Using a Topological Index Method. *Ind. Eng. Chem. Res.* 2014, *53* (17), 7224−7232.
(62) Wu, K.-J.; Chen, Q.-L.; He, C.-H. Speed of sound of ionic liquids: Database, estimation, and its application for thermal conductivity prediction. *AIChE J.* 2014, *60* (3), 1120−1131.
(63) Wu, K.-J.; Zhao, C.-X.; He, C.-H. Development of a group contribution method for determination of thermal conductivity of ionic liquids. *Fluid Phase Equilib.* 2013, *339*, 10−14.
(64) Gardas, R. L.; Coutinho, J. A. P. Group contribution methods for the prediction of thermophysical and transport properties of ionic liquids. *AIChE J.* 2009, *55* (5), 1274−1290.
(65) Gardas, R. L.; Ge, R.; Goodrich, P.; Hardacre, C.; Hussain, A.; Rooney, D. W. Thermophysical Properties of Amino Acid-Based Ionic Liquids. *J. Chem. Eng. Data* 2010, *55* (4), 1505−1515.
(66) Hezave, A. Z.; Raeissi, S.; Lashkarbolooki, M. Estimation of Thermal Conductivity of Ionic Liquids Using a Perceptron Neural Network. *Ind. Eng. Chem. Res.* 2012, *51* (29), 9886−9893.
(67) Koller, T. M.; Schmid, S. R.; Sachnov, S. J.; Rausch, M. H.; Wasserscheid, P.; Fröba, A. P. Measurement and Prediction of the Thermal Conductivity of Tricyanomethanide- and Tetracyanoborate-Based Imidazolium Ionic Liquids. *Int. J. Thermophys* 2014, *35* (2), 195−217.
(68) Nieto De Castro, C. A.; Lourenço, M. J. V.; Ribeiro, A. P. C.; Langa, E.; Vieira, S. I. C.; Goodrich, P.; Hardacre, C. Thermal Properties of Ionic Liquids and IoNanofluids of Imidazolium and Pyrrolidinium Liquids. *J. Chem. Eng. Data* 2010, *55* (2), 653−661.
(69) Oster, K.; Goodrich, P.; Jacquemin, J.; Hardacre, C.; Ribeiro, A. P. C.; Elsinawi, A. A new insight into pure and water-saturated quaternary phosphonium-based carboxylate ionic liquids: Density, heat capacity, ionic conductivity, thermogravimetric analysis, thermal conductivity and viscosity. *J. Chem. Thermodyn.* 2018, *121*, 97−111.
(70) Rodil, E.; Arce, A.; Arce, A.; Soto, A. Measurements of the density, refractive index, electrical conductivity, thermal conductivity and dynamic viscosity for tributylmethylphosphonium and methyl-sulfate based ionic liquids. *Thermochim. Acta* 2018, *664*, 81−90.
(71) Valkenburg, M. E. V.; Vaughn, R. L.; Williams, M.; Wilkes, J. S. Thermochemistry of ionic liquid heat-transfer fluids. *Thermochim. Acta* 2005, *425* (1−2), 181−188.
(72) Zaripov, Z. I.; Gumerov, F. M.; Khairutdinov, V. F.; Małgorzata, M.; Edward, Z.; Marzena, D.; Abdulagatov, I. M. Thermal conductivity and thermal diffusivity of Pyrrolidinium-BasedIonic liquids at atmospheric pressure. *Fluid Phase Equilib.* 2019, *485*, 135−145.
(73) Tenney, C. M.; Massel, M.; Mayes, J. M.; Sen, M.; Brennecke, J. F.; Maginn, E. J. A Computational and Experimental Study of the Heat Transfer Properties of Nine Different Ionic Liquids. *J. Chem. Eng. Data* 2014, *59* (2), 391−399.
(74) Yebra, F.; Troncoso, J.; Romaní, L. Thermal conductivity of ionic liquids under pressure. *Fluid Phase Equilib.* 2020, *515*, 112573.
(75) Tomida, D.; Kenmochi, S.; Tsukada, T.; Qiao, K.; Yokoyama, C. Thermal Conductivities of [bmim][PF_6], [hmim][PF_6], and [omim][PF_6] from 294 to 335 K at Pressures up to 20 MPa. *Int. J. Thermophys* 2007, *28* (4), 1147−1160.
(76) Huber, M. L. Models for Viscosity, Thermal Conductivity, and Surface Tension of Selected Pure Fluids as Implemented in REFPROP v10.0. *NISTIR 8209*; 2018.
(77) Perkins, R. A.; Huber, M. L. Measurement and Correlation of the Thermal Conductivity of Pentafluoroethane (R125) from 190 to 512 K at Pressures to 70 MPa. *J. Chem. Eng. Data* 2006, *51* (3), 898−904.
(78) Perkins, R. A.; Laesecke, A.; Howley, J.; Ramires, M. L. V.; Gurova, A. N.; Cusco, L. Experimental Thermal Conductivity Values for the IUPAC Round Robin Sample of 1,1,1,2-Tetrafluoroethane (R134a). *NISTIR 6605*; 2000.
(79) Tomida, D.; Kenmochi, S.; Tsukada, T.; Qiao, K.; Yokoyama, C. Thermal Conductivities of Imidazolium-based Ionic Liquid + CO_2 Mixtures. *Int. J. Thermophys* 2010, *31* (10), 1888−1895.
(80) Rausch, M. H.; Heller, A.; Herbst, J.; Koller, T. M.; Bahlmann, M.; Schulz, P. S.; Wasserscheid, P.; Fröba, A. P. Mutual and Thermal Diffusivity of Binary Mixtures of the Ionic Liquids [BMIM][$C(CN)_3$] and [BMIM][$B(CN)_4$] with Dissolved CO_2 by Dynamic Light Scattering. *J. Phys. Chem. B* 2014, *118* (17), 4636−4646.
(81) Klein, T.; Piszko, M.; Lang, M.; Mehler, J.; Schulz, P. S.; Rausch, M. H.; Giraudet, C.; Koller, T. M.; Fröba, A. P. Diffusivities in Binary Mixtures of [AMIM][NTf_2] Ionic Liquids with the Dissolved Gases H_2, He, N_2, CO, CO_2, or Kr Close to Infinite Dilution. *J. Chem. Eng. Data* 2020, *65* (8), 4116−4129.
(82) Kian, K.; Scurto, A. M. Heat Transport Properties of CO_2-Expanded Liquids:n-Hexane,n-Decane, and n-Tetradecane. *Ind. Eng. Chem. Res.* 2017, *56* (44), 12822−12832.
(83) Al-Barghouti, K. S.; Scurto, A. M. Thermal Conductivity of the Ionic Liquid [HMIm][Tf_2N] with Compressed Carbon Dioxide. *AIChE J.* 2022, *68*, e17635.
(84) Ren, W.; Scurto, A. M. Global Phase Behavior of Imidazolium Ionic Liquids and Compressed 1,1,1,2-Tetrafluoroethane (R-134a). *AIChE J.* 2009, *55* (2), 486−493.
(85) Ren, W.; Scurto, A. M. Phase equilibria of imidazolium ionic liquids and the refrigerant gas, 1,1,1,2-tetrafluoroethane (R-134a). *Fluid Phase Equilib.* 2009, *286* (1), 1−7.

https://doi.org/10.1021/acs.jced.2c00054
J. Chem. Eng. Data XXXX, XXX, XXX−XXX

(86) Ahosseini, A.; Scurto, A. M. Viscosity of imidazolium-based ionic liquids at elevated pressures: Cation and anion effects. *Int. J. Thermophys* 2008, *29* (4), 1222−1243.
(87) Morais, A. R. C.; Alaras, L. M.; Baek, D. L.; Fox, R. V.; Shiflett, M. B.; Scurto, A. M. Viscosity of 1-Alkyl-1-methylpyrrolidinium Bis(trifluoromethylsulfonyl)imide Ionic Liquids Saturated with Compressed CO_2. *J. Chem. Eng. Data* 2019, *64* (11), 4658−4667.
(88) Roder, H. M. A Transient Hot Wire Thermal Conductivity Apparatus for Fluids. *J. Res. Natl. Inst. Stand. Technol.* 1981, *86* (5), 457−493.
(89) Cohen, E.; Glicksman, L. Analysis of the Transient Hot-Wire Method to Measure Thermal Conductivity of Silica Aerogel: Influence of Wire Length, and Radiation Properties. *J. Heat Transfer* 2014, *136* (4), 041301.
(90) Assael, M. J.; Karagiannidis, L.; Malamataris, N.; Wakeham, W. A. *Int. J. Thermophys* 1998, *19* (2), 379−389.
(91) Kian, K. Modelling of Phase Behavior and Transport Properties of Compressed CO_2-Saturated Alkanes: CO_2/n-Hexane, CO_2/n-Decane, and CO_2/n-Tetradecane. MS Thesis, University of Kansas, 2017.
(92) Nwosu, S. *Environmentally Benign Production of Ionic Liquids in CO_2-Expanded Systems*; Ph.D. Dissertation, University of Kansas: 2012.
(93) NIST Standard Reference Database 23: Reference Fluid Thermodynamic and Transport Properties-REFPROP, version 10.0; National Institute of Standards and Technology, Standard Reference Data Program, Gaithersburg, MD; 2018 (accessed 2021).
(94) Assael, M. J.; Bogdanou, I.; Mylona, S. K. Reference Correlation of the Thermal Conductivity of n-Heptane from the Triple Point to 600 K and up to 250 MPa. *J. Phys. Chem. Ref. Data* 2013, *42* (2), 023101.
(95) Assael, M. J.; Charitidou, E.; Castro, C. A. N. d.; Wakeham, W. A. The Thermal Conductivity of n-Hexane, n-Heptane, and n-Decane by the Transient Hot-Wire Method. *Int. J. Thermophys.* 1987, *8*, 663−670.
(96) Castro, C. A. N. d.; Calado, J. C. G.; Wakeham, W. A.; Dix, M. An apparatus to measure the thermal conductivity of liquids. *J. Phys. E: Sci. Instrum.* 1976, *9* (12), 1073−1080.
(97) Nagasaka, Y.; Nagashima, A. Precise measurements of the thermal conductivity of toluene and n-heptane by the absolute transient hot-wire method. *Ind. Eng. Chem. Fundam.* 1981, *20* (3), 216−220.
(98) Qun-Fang, L.; Rui-Sen, L.; Dan-Yan, N.; Yu-Chun, H. Thermal Conductivities of Some Organic Solvents and Their Binary Mixtures. *J. Chem. Eng. Data* 1997, *42* (5), 971−974.
(99) Antoniadis, K. D.; Tertsinidou, G. J.; Assael, M. J.; Wakeham, W. A. Necessary Conditions for Accurate, Transient Hot-Wire Measurements of the Apparent Thermal Conductivity of Nanofluids are Seldom Satisfied. *Int. J. Thermophys* 2016, *37*, No. 78.
(100) Ramires, M. L. V.; Nieto De Castro, C. A. Standard Reference Data for the Thermal Conductivity of Water. *J. Phys. Chem. Ref. Data* 1995, *24* (3), 1377−1381.
(101) Makino, T.; Kanakubo, M.; Masuda, Y.; Umecky, T.; Suzuki, A. CO_2 absorption properties, densities, viscosities, and electrical conductivities of ethylimidazolium and 1-ethyl-3-methylimidazolium ionic liquids. *Fluid Phase Equilib.* 2014, *362*, 300−306.
(102) Zhang, W.; Chen, X.; Wang, Y.; Wu, L.; Hu, Y. Experimental and Modeling of Conductivity for Electrolyte Solution Systems. *ACS Omega* 2020, *5* (35), 22465−22474.
(103) Menashe, J.; Wakeham, W. A. Absolute Measurements of the Thermal Conductivity of Liquids at Pressures up to 500 MPa. *Ber. Bunsen. Phys. Chem.* 1981, *85* (4), 340−347.
(104) Ren, W.; Scurto, A. M.; Shiflett, M. B.; Yokozeki, A. Phase Behavior and Equilibria of Ionic Liquids and Refrigerants: 1-Ethyl-3-methyl-imidazolium Bis(trifluoromethylsulfonyl)imide ([EMIm]-[Tf2N]) and R-134a. In *Gas-Expanded Liquids and Near-Critical Media*; Hutchenson, K. W., Scurto, A. M., Subramaniam, B., Eds.; American Chemical Society: 2009; Vol. *1006*, pp 112−128.
(105) Valderrama, J. O.; Rojas, R. E. Critical Properties of Ionic Liquids. Revisited. *Ind. Eng. Chem. Res.* 2009, *48* (14), 6890−6900.
(106) Valderrama, J. O.; Forero, L. A.; Rojas, R. E. Critical Properties and Normal Boiling Temperature of Ionic Liquids. Update and a New Consistency Test. *Ind. Eng. Chem. Res.* 2012, *51* (22), 7838−7844.
(107) Valderrama, J. O.; Robles, P. A. Critical Properties, Normal Boiling Temperatures, and Acentric Factors of Fifty Ionic Liquids. *Ind. Eng. Chem. Res.* 2007, *46* (4), 1338−1344.
(108) Lydersen, A. L. Estimation of Critical Properties of OrganicCompounds. Report 3; University of Wisconsin: Madison, WI, 1955.
(109) Joback, K. G.; Reid, R. C. Estimation of Pure-Component Properties from Group-Cntributions. *Chem. Eng. Commun.* 1987, *57* (1−6), 233−243.
(110) Tillner-Roth, R.; Baehr, H. D. An International Standard Formulation for the Thermodynamic Properties of 1,1,1,2-Tetrafluoroethane (HFC-134a) for Temperatures from 170 to 455 K and Pressures up to 70 MPa. *J. Phys. Chem. Ref. Data* 1994, *23*, 657.
(111) Sandler, S. I. *Chemical, Biochemical, and Engineering Thermodynamics*; Wiley: 2017.
(112) Smith, F. L.; Harvey, A. H. Avoid Common Pitfalls When Using Henry's Law. *Chemical Engineering Progress*; 2007; https://tsapps.nist.gov/publication/get_pdf.cfm?pub_id=50449.
(113) Tariq, M.; Serro, A. P.; Mata, J. L.; Saramago, B.; Esperança, J. M. S. S.; Canongia Lopes, J. N.; Rebelo, L. P. N. High-temperature surface tension and density measurements of 1-alkyl-3-methylimidazolium bistriflamide ionic liquids. *Fluid Phase Equilib.* 2010, *294* (1−2), 131−138.
(114) Seoane, R. G.; Corderí, S.; Gómez, E.; Calvar, N.; González, E. J.; Macedo, E. A.; Domínguez, A. Temperature Dependence and Structural Influence on the Thermophysical Properties of Eleven Commercial Ionic Liquids. *Ind. Eng. Chem. Res.* 2012, *51* (5), 2492−2504.
(115) Paulechka, Y. U.; Blokhin, A. V.; Kabo, G. J.; Strechan, A. A. Thermodynamic properties and polymorphism of 1-alkyl-3-methylimidazolium bis(triflamides). *J. Chem. Thermodyn.* 2007, *39* (6), 866−877.
(116) van Konynenburg, P. H.; Scott, R. L. Critical lines and phase equilibria in binary van der Waals mixtures. *Philos. Trans R Soc. London Ser. A* 1980, *298*, 495−540.
(117) Muldoon, M. J.; Aki, S. N. V. K.; Anderson, J. L.; Dixon, J. K.; Brennecke, J. F. Improving Carbon Dioxide Solubility in Ionic Liquids. *J. Phys. Chem. B* 2007, *111* (30), 9001−9009.
(118) Almantariotis, D.; Gefflaut, T.; PáDua, A. A. H.; Coxam, J. Y.; Costa Gomes, M. F. Effect of Fluorination and Size of the Alkyl Side-Chain on the Solubility of Carbon Dioxide in 1-Alkyl-3-methylimidazolium Bis(trifluoromethylsulfonyl)amide Ionic Liquids. *J. Phys. Chem. B* 2010, *114* (10), 3608−3617.
(119) Gutkowski, K. I.; Shariati, A.; Peters, C. J. High-pressure phase behavior of the binary ionic liquid system 1-octyl-3-methylimidazolium tetrafluoroborate+carbon dioxide. *J. Supercrit. Fluids* 2006, *39* (2), 187−191.
(120) Liu, X.; O'Harra, K. E.; Bara, J. E.; Turner, C. H. Molecular insight into the anion effect and free volume effect of CO_2 solubility in multivalent ionic liquids. *Phys. Chem. Chem. Phys.* 2020, *22* (36), 20618−20633.
(121) Shannon, M. S.; Tedstone, J. M.; Danielsen, S. P. O.; Hindman, M. S.; Irvin, A. C.; Bara, J. E. Free Volume as the Basis of Gas Solubility and Selectivity in Imidazolium-Based Ionic Liquids. *Ind. Eng. Chem. Res.* 2012, *51* (15), 5565−5576.
(122) May, E. F.; Moldover, M. R.; Schmidt, J. W. The Dielectric Permittivity of Saturated Liquid Carbon Dioxide and Propane Measured Using Cross Capacitors. *Int. J. Thermophys* 2005, *26* (3), 563−576.
(123) Gbur, A. M.; Johnson, P. Determination of dielectric properties of refrigerants. *ASHRAE Trans.* 2005, *111*, 26−36.
(124) Chen, Q.-L.; Wu, K.-J.; He, C.-H. Thermal Conductivities of [EMIM][$EtSO_4$], [EMIM][$EtSO_4$] + C_2H_5OH, [EMIM][$EtSO_4$] +

https://doi.org/10.1021/acs.jced.2c00054
J. Chem. Eng. Data XXXX, XXX, XXX−XXX

H_2O, and [EMIM][$EtSO_4$] + C_2H_5OH + H_2O at T = (283.15 to 343.15) K. *J. Chem. Eng. Data* 2013, *58* (7), 2058−2064.

https://doi.org/10.1021/acs.jced.2c00054
J. Chem. Eng. Data XXXX, XXX, XXX−XXX